THE ASTROPHYSICAL JOURNAL, 492:511–520, 1998 January 10

MODELING THE CONTINUUM AND LINE SPECTRA OF THE SEYFERT 2 GALAXY NGC 5252

M. CONTINI,[1] M. A. PRIETO,[2] AND S. M. VIEGAS[3]
Received 1996 November 25; accepted 1997 August 22

ABSTRACT

The S0 galaxy NGC 5252 is one of the best examples of the anisotropic radiation theories believed to govern the physics of active galactic nuclei. Considerable amounts of observational data, from the radio to the hard X-ray domain, have been accumulated from the central nuclear region of this galaxy. This work makes use of all the available observational information in an attempt to model in a self-consistent manner the continuum and line emission spectra of the nuclear region and the extended emission-line region.

It is suggested that both the nuclear continuum and the nuclear line emission originate in gaseous clouds that are exposed to the nuclear ionizing radiation and subjected to shocks. The best fit to the data in the nuclear region is obtained with a weighted-average model that includes radiation-dominated clouds with low velocities ($\simeq 100$ km s^{-1}), producing most of the emission lines and the low-frequency continuum, and high-velocity (~ 400 km s^{-1}) shock-dominated clouds, where the soft X-ray continuum originates. The far-infrared emission is due to dust heated by both the nuclear radiation and shocks.

Modeling of the extended emission-line region was performed on the basis of the derived nuclear model. That region was found to be characterized by densities of a few cm^{-3} and a cloud size of about 100 pc. Excitation via shocks is found negligible, whereas photoionization by the central power source widely accounts for the observed line spectrum.

Subject headings: galaxies: active — galaxies: individual (NGC 5252) — galaxies: Seyfert — radiation mechanisms: thermal — X-rays: galaxies

1. INTRODUCTION

The interpretation and modeling of the narrow-line region in active galactic nuclei (AGNs) has been, since the early 1980s, a very active topic of study. Photoionization models, designed for planetary nebulae and H II regions, have been the most basic tool for interpreting AGN spectra. But as observations across the electromagnetic spectrum have gained in quality and line richness, it has been realized that photoionization alone cannot account for the full range of observed line strengths. Multiple-density models were invoked by many authors (e.g., Filippenko 1985; Viegas-Aldrovandi & Gruenwald 1988). Viegas-Aldrovandi & Gruenwald (1988) analyzed several diagnostic diagrams and showed that, in particular, these models cannot resolve the problem of fitting the strong high-level lines (e.g., [Fe X]).

An additional heating mechanism seems to be required (for a review on the topic see Viegas & Contini 1997). Shock heating appears to be the most promising mechanism coupled with photoionization, particularly in view of the jets associated with emission-line regions and of the direct detection of shock fronts in *Hubble Space Telescope HST* images of the NLR in Seyfert galaxies (Pogge 1997). The coupled effect of shocks and photoionization was strongly favored by Viegas & Contini in their series of papers (see Viegas & Contini 1994, hereafter VC94, and references therein) and recently by Sutherland, Bicknell, & Dopita (1993). The key issue of whether both the nuclear and the extended NLR in AGNs are powered by photoionization, shocks, or both has been hotly debated in the last few years (e.g., Morse, Raymond, & Wilson 1996; Ho, Filippenko, & Sargent 1993; Binette, Wilson, & Storchi-Bergmann 1996). The usual way to discriminate between the various mechanisms is through the use of line-ratio diagnostic diagrams. Essentially, AGN spectra are classified by their location in the diagnostic diagrams, where the observed line ratios are compared with model calculations. This comparison provides information on the physical conditions of the emitting gas as well as on the ionization mechanism.

There are, however, several drawbacks to this general approach. First, objects are anonymously represented in the diagrams, and consistency of the results derived from individual data points is in general not checked. Second, diagnosis is exclusively based on the behavior of optical lines (e.g., Baldwin, Phillips, & Terlevich 1981; Veilleux & Osterbrock 1987; Viegas-Aldrovandi & Gruenwald 1988). Emission coronal lines are usually investigated separately (e.g., Korista & Ferland 1989) without special concern about consistency with the other optical-line results.

In the few studies of single identified objects (e.g., Binette et al. 1996) some incoherences between different diagrams were discussed. As for model calculations, Dopita & Sutherland (1995, 1996), in an attempt to include the combined effect of photoionization and shocks, produced a grid of low-density shock models in which the effect of the post-shock diffuse radiation is accounted for. However, these models are still pure shock models, as the main photoionization source, that from the active nucleus, has not been included.

The present paper attempts to overcome some of the drawbacks mentioned above by performing a simultaneous modeling of the line and continuum spectra of a given object using the maximum possible energy coverage. To this

[1] School of Physics and Astronomy, Tel-Aviv University, Ramat-Aviv, Tel Aviv 69978, Israel.
[2] Max-Planck-Institut für extraterrestrische Physik, D-85748 Garching, Germany.
[3] Instituto Astronômico e Geofísico, USP, avenida Miguel Stefano 4200, 04301, São Paulo, SP, Brazil.

end, model calculations that include the combined effect of shocks, induced photoionization by shocks, *and* photoionization by the central source are used (the last version of the models, code SUMA, is in VC94). The models also include a self-consistent treatment of the effect of dust, including reciprocal heating and cooling of dust and gas and sputtering of the grains. The dust treatment is based on previous works by Draine (1981), Dwek (1981, 1988), and J. M. Greenberg (1992, private communication).

The modeling was applied to the Seyfert 2 galaxy NGC 5252. This object was selected for the following reasons: First, it shows one of the best examples of radiation anisotropy among AGNs, and the interpretation of its nuclear spectrum thus becomes of general interest for the Seyfert class. Second, a large body of observational data, from hard X-rays to radio waves, has been accumulated for both the nuclear and the extended emission-line regions and can be used for modeling purposes. Finally, no evidence for circumnuclear star formation activity is apparent in this S0 galaxy, which largely simplifies both modeling and interpretation of the nuclear spectrum.

In this work we make use of all the available observational information in an attempt to produce a self-consistent representation of both continuum and line spectra in the nuclear and extended emission-line region of NGC 5252. Section 2 presents a general description of the shock plus photoionization composite models. Section 3 reviews the current state of knowledge for NGC 5252, and § 4 presents the observational data used in the analysis. The model results are discussed in §§ 5 and 6. Conclusions follow in § 7.

2. SHOCK PLUS PHOTOIONIZATION MODELS: GENERAL DESCRIPTION

The continuum and emission-line spectra of NGC 5252 are analyzed using a composite model for the narrow-line region (NLR). In our model the clouds move radially outward from the active center, and a shock forms on the outer edge of the clouds. The photon flux from the active source reaches the clouds on the inner edge opposite the shock front. The SUMA code (VC94) is adapted to calculate the emission spectra (lines and continuum) from a *shocked cloud that may also be affected by photoionizing radiation from the central source.* This code consistently calculates shock and radiation effects in a plane-parallel geometry.

Shocked gas in the immediate postshock region can reach temperatures higher than 10^6 K for shock velocities $V_s \geq 300$ km s^{-1}. X-ray emission at energies higher than 0.1 keV is produced, the X-ray flux increasing rapidly with V_s (cf. VC94). On the other hand, the photoionizing flux is particularly efficient downstream, keeping the downstream gas at temperatures of $\sim 10^4$ K in a large region (cf. Contini & Aldrovandi 1983). Therefore, stronger lines of intermediate ionization levels correspond to stronger ionizing fluxes. The temperature of the gas drops downstream to $T_e \ll 10^4$ K as the result of cooling by free-free and free-bound continuum emission, line emission, and emission from dust. A region with temperature between 10^3 and 10^4 K may be present owing to the diffuse radiation emitted from the hot gas zone. The low-temperature gas is particularly responsible for the emission of neutral lines and for the radio bremsstrahlung.

The IR emission by dust present in the cloud is also calculated by SUMA. The IR bumps are due to emission from dust grains that are heated by radiation and collisions at the shock front. Grain cooling rates are obtained from the Planck-averaged value of the absorption coefficients, assuming that each grain emits as a blackbody (cf. Viegas & Contini 1994, § 3). The final spectrum is the integration of the dust emission over the different grain temperatures in the cloud.

The input parameters to the model are the shock velocity, V_s, the preshock density n_0, the magnetic field B_0, and the ionizing radiation spectrum, which is characterized by the flux at the Lyman limit F_H, the high-energy cutoff E_c, and the spectral index α. The amount of dust is given by the parameter d/g, the dust-to-gas number ratio. Cosmic gas abundances from Allen (1973) are used.

Some general results raising from our previous analysis of the NLR by SUMA help to set limits to some of the above input parameters:

1. The values of F_H and V_s determine the type of model, i.e., radiation dominated (RD) or shock dominated (SD).
2. RD models show emission-line intensities similar to those produced by pure photoionization models. Thus, for cosmic abundances the calculated gas temperature is less than 2×10^4 K, and the RD clouds contribute only to the IR-optical emission.
3. Both soft X-rays and high-ionization emission lines like [Fe VII], [Fe X], and [Ne V] are produced in the postshock zones of high-velocity SD clouds.
4. The higher the shock velocity, the higher the temperature in the postshock zone, leading to a *continuum distribution peaked in the UV–soft X-ray band.*
5. The intensity of the IR continuum determines the dust-to-gas ratio. The frequency at which the IR continuum peaks increases with the shock velocity.
6. Clouds with geometrical thickness $D < 10^{18}$ cm absorb most of the ionizing radiation from the central source; only high-energy photons ($E > 0.5$ keV) can escape from the cloud.
7. The magnetic field B_0 is related to the cloud compression. Changes in B_0 imply variations in the preshock density n_0: a lower B_0 corresponds to a higher I_0. A magnetic field $B_0 \sim 10^{-4}$ G was found in Contini & Aldrovandi (1986) to be a suitable value for the NLR clouds.
8. The higher the value of the high-energy cutoff, E_c, the wider the transition zone in the cloud. The transition zone is defined as the region where hydrogen is half-ionized and ions in the lower ionization states are present.

3. NGC 5252

NGC 5252 is an S0 galaxy at a redshift of $z \simeq 0.0230$. It has an optical size of $\sim 1'.4 \times 0'.9$, with the major axis at a position angle P.A. $\sim 15°$. NGC 5252 harbors a Seyfert 2 nucleus which illuminates a remarkably well-defined biconical structure of ionized gas extending up to 17 kpc ($H_0 = 100$ km s^{-1} Mpc^{-1}; $1''$ corresponds to 335 pc) from the center of the galaxy (Tadhunter & Tsvetanov 1989). In addition, an equivalent region of neutral gas fills the regions outside the ionization bicone (Prieto & Freudling 1993).

Accumulated observations at different spectral bands have provided important constraints on the nature of the nuclear region in this object. Some of them are summarized below; They were used in modeling the radiation field in this galaxy.

The gas kinematics in the central region of NGC 5252 are complex. Both neutral and ionized gas present a rather distorted, though similar, rotation pattern with a total amplitude velocity of ~ 200 km s^{-1} with respect to the systemic velocity (Prieto & Freudling 1996). Clear departures from rotation are seen at different locations, in particular in the very central region where velocities can rise up to 300 km s^{-1}. Within the inner few arcseconds, the ionized gas shows double-peaked profiles and is counterrotating with respect to the galactic stellar body (Held, Cappaccioli, & Cappellaro 1992).

NGC 5252 does not show ongoing star formation in its disk. Deep Hα imaging of the galaxy (Prieto & Freudling 1996) reveals the H II gas to be confined within the ionization bicone. The observed emission from the ionization bicone may thus be linked to the central power source.

Combined near-IR and optical imaging of NGC 5252 point out the presence of a heavily obscured AGN nucleus (Kotilainen & Prieto 1995). A band of red material lying across the nucleus perpendicular to the bicone of ionized gas is detected in the IR/optical ratio maps. The presence of an obscured nucleus is also confirmed in the high-energy domain. The 0.4–10 keV *ASCA* spectrum of the galaxy (Cappi et al. 1996) reveals a heavily obscured nucleus with $N(\mathrm{H}) \sim 4.3 \times 10^{22}$ cm^{-2}. This implies about 20 mag extinction in the visible, sufficient to absorb all the optical and UV nuclear light in the line of sight.

The 2–10 keV region is well characterized by a relatively flat power-law spectrum with spectral index $\alpha \sim -0.45 \pm 0.2$. However, the extrapolation of this spectrum to the soft X-ray region reveals an additional soft excess component at about 1 keV.

4. OBSERVATIONS

Data on the nuclear continuum energy distribution of NGC 5252 have mostly been taken from Kotilainen & Prieto (1995) and references therein, and include data from radio, far-IR (*IRAS*), near-IR, optical, and UV bands. This continuum data set was complemented with a new data point at 10 μm which corresponds to the integrated nuclear flux within a 5.″3 aperture (Maiolino et al. 1995). The nonstellar nuclear continuum fluxes derived by Kotilainen & Prieto (1995) in the near-IR to optical range are considered for comparison purposes. Upper limits to the nuclear continuum light are available in the UV (the UV continuum of NGC 5252 was undetected in a 9 hr of *IUE* exposure of the galaxy) and in the millimeter region (Prieto & Freudling 1996). The hard (1–10 keV) X-ray spectrum of NGC 5252 was taken from Cappi et al. (1996), who fitted a power-law model with $\alpha = -0.45$ and $N(\mathrm{H}) = 4.3 \times 10^{22}$ cm^{-2} to the *ASCA* spectrum of the galaxy.

The central optical nebular emission was taken from the high-dispersion nuclear spectrum by Osterbrock & Martel (1993), which corresponds to a 2.″1 × 5″ aperture centered on the nucleus. The reported line fluxes were derived after removal of the stellar contribution and then reddening corrected. They are listed in Table 1, column (3).

The data of Osterbrock & Martel (1993) were complemented with more recent nuclear spectroscopy by Acosta-Pulido et al. (1996). In the latter case, the nuclear fluxes are integrated within a smaller, 2.″8 × 1.″8, aperture; yet the derived line ratios are within the errors in fair agreement with the results of Osterbrock & Martel (1993). Acosta-Pulido et al. (1996) provide two sets of data, one corresponding to fluxes derived before the removal of the stellar contribution. These have been reddening corrected and are given in column (2) of Table 1. The second set corresponds to the line fluxes after the stellar removal, and is listed in column (3) of Table 1 (indicated by the asterisks).

The gas within the NGC 5252 bicone corresponding to different extended emission-line regions was modeled using the highest signal-to-noise optical spectra by Acosta-Pulido et al. (1996).

5. MODELING THE NUCLEAR REGION OF NGC 5252

5.1. *Setting the Model Parameters*

Table 1 lists the observed emission-line fluxes relative to Hβ. Different model results are presented and will be discussed in §§ 5.2 and 5.3.

Line ratios such as [O III] λ5007+/Hβ, [O III] λ5007+/[O II] λ3727+, He II/Hβ, [O I] λ6300+/Hβ, [O III] λ5007+/[O III] 4363 ($=R_{[\mathrm{O\ III}]}$), [Fe X]/Hβ, [Ne V]/Hβ, and [S II] λ6717/[S II] λ6730 (the plus sign indicates that the doublet is considered) are particularly important, as they strongly constrain the models. The observed [O III] λ5007+/Hβ, [O III]/[O II], and He II/Hβ ratios indicate that the spectrum is radiation dominated and that the intensity of the ionizing flux from the active center is moderately low, i.e., $F_{\mathrm{H}} < 10^{10}$ photons cm^{-2} s^{-1} eV^{-1} at 1 rydberg (cf. Viegas-Aldrovandi & Contini 1989) and the relatively high [O I]/Hβ line ratio indicates a high high-energy cutoff ($E_c > 10^3$ eV).

Except for the [Fe X], [Ne V], and [O III] λ4363 line ratios, the remaining line ratios, and in particular He II λ4686/Hβ , are consistent with an ionizing spectrum with spectral index α of the order of 1.5 ($F_\nu \propto \nu^{-\alpha}$) and intensity $F_{\mathrm{H}} = 4 \times 10^9$ photons cm^{-2} s^{-1} eV^{-1} at 1 rydberg. On the other hand, the X-ray observations of NGC 5252 indicate a flatter spectrum ($\alpha_{\mathrm{X}} \simeq 0.4$ at energies above 1 keV). If such a flat spectrum is extrapolated to lower energies, the resulting ionizing spectrum becomes insufficient to account for the observed optical line ratios. Within a reasonable range of sizes for the NLR, 10–10^3 pc, a power-law extrapolation to 1 rydberg with $\alpha_{\mathrm{X}} = 0.4$ yields a Lyman flux $F_{\mathrm{H}} \simeq 2 \times 10^6$ cm^{-2} s^{-1} eV^{-1}, which is too low. Thus, if the continuum emission at $E \geq 1$ keV originates entirely at the central source, a composite spectrum for the ionizing radiation should be assumed. A combination of two power laws with indices $\alpha_{\mathrm{X}} = 0.4$ and $\alpha_{\mathrm{UV}} = 1.5$ and $E_c > 5$ keV was assumed as the ionizing radiation spectrum. AGN spectra with composite spectral indices have been observed and discussed (e.g., Mushotzky 1982; Stein 1988).

It is also assumed that the observed continuum emission at 1 keV is in its totality due to the central source and that the transition between the two power laws occurs at $E_{\mathrm{X}} = 260$ eV.

The composite ionizing radiation spectrum is given by $F(E) = F_{\mathrm{H}}(13.6/E)^{2.5}$ for $E \leq E_{\mathrm{X}}$, and $F(E) = F_{\mathrm{X}}(13.6/E)^{1.4}$ for $E \geq E_{\mathrm{X}}$, where $F_{\mathrm{H}}$and F_{X} are normalized to the observed flux at 1 keV (1.96×10^{-6} cm^{-2} s^{-1} eV^{-1}; Cappi et al. 1996) as follows: $F(1\ \mathrm{keV}) = F_{\mathrm{X}}(13.6 \times 10^{-3})^{1.4} = 1.96 \times 10^{-6}(\Delta/r)^2$, and $F_{\mathrm{H}} = F_{\mathrm{X}}(13.6/E_{\mathrm{X}})^{1.4}(E_{\mathrm{X}}/13.6)^{2.5}$.

Assuming $E_{\mathrm{X}} = 260$ eV, the distance Δ to NGC 5252 is 70 Mpc, and a range of distances for the NLR clouds to the central source between 0.1 and 1 kpc, the derived F_{H} values range from 10^8 to 10^{10} cm^{-2} s^{-1} eV^{-1}.

Note that the postulated composite ionizing continuum

TABLE 1

NUCLEAR EMISSION-LINE SPECTRUM

Line/Parameter (1)	Observation (2)	Observation (Stellar Subtracted) (3)	R1 (4)	R2 (5)	R3 (6)	S1 (7)	S2 (8)	S1 + S2 (9)	AV1 (10)	AV2 (11)	AV3 (12)
[Ne v] λ3426	0.58	...	0.002	0.62	0.03	3.60	0.06	2.06	0.50	0.50	0.02
[O II] λ3727+	5.80	3.00*	5.60	4.30	0.08	10.0	2.00	6.54	6.50	4.70	5.64
[Ne III] λ3869+	1.18	1.30*	1.18	1.80	0.85	2.47	0.72	1.70	1.40	1.20	1.19
[S II] λ4069+	0.31	0.42*	0.26	1.34	0.00	0.60	0.85	0.71	0.32	0.35	0.28
[O III] λ4363	0.61	0.24*	0.04	0.81	0.29	1.00	0.02	0.58	0.20	0.20	0.07
He II λ4686	...	0.16	0.17	0.06	0.70	0.23	0.10	0.17	0.19	0.23	0.17
[O III] λ5007+	...	9.2	9.45	9.40	21.0	13.9	0.71	8.19	10.6	10.9	9.50
[N I] λ5199+	...	0.16	0.23	0.80	0.00	0.56	0.07	0.35	0.29	0.26	0.23
[O I] λ6300+	...	1.72	1.72	7.60	0.00	3.00	2.00	2.56	2.00	2.20	1.72
[Fe X] λ6375	...	0.02	0.00	0.00	0.03	1.87	0.54	1.29	0.20	0.01	0.01
[N II] λ6548+	...	3.57	4.20	4.80	0.00	4.20	4.70	4.40	4.20	3.70	4.50
[S II] λ6717+	...	2.50	4.00	4.40	0.00	3.50	1.00	2.60	3.90	3.50	4.00
[S II] λ6717/[S II] λ6731	...	1.13	1.10	0.60	...	0.75	0.46	0.62	1.07	0.89	1.10
Hβ absorption (ergs cm^{-2} s^{-1})	...	...	0.016	0.005	1.0	0.0011	0.21	...	...	...	...
V_s (km s^{-1})	...	...	100	140	100	450	1000	...	...	...	...
n_0 (cm^{-3})	...	...	100	2000	100	200	300	...	...	...	...
F_H (10^9 cm^{-2} s^{-1} eV^{-1})	...	...	4	5	60	...	...	...	...	...	...
U	...	...	1.3(−4)	3.3(−6)	2(−3)	...	...	...	...	...	...
d/g (10^{-15})	...	...	2	0.5	0.1	10	20	...	...	...	...
D (10^{18} cm)	...	...	1.5	0.5	2	>0.2	>29	...	...	...	...
W1	...	...	1	...	...	2	...	...	...	...	...
W2	...	...	100	50	0.3	5	...	...	...	...	...
W3	...	...	100	...	...	5.	0.02	...	...	...	...

NOTE—Comparison of model calculations with observations. U is the ionization parameter calculated at the photoionization edge. For all models a magnetic field $B_0 = 10^{-4}$ G is adopted. The spectral index in the UV adopted from previous calculations for AGNs ($\alpha_{UV} = 1.5$) is confirmed by the fit of the He II λ4686/Hβ line ratio. The spectral index in the X-ray region ($\alpha_X = 0.4$) is taken from the observations.

is assumed to be fully absorbed below 1 keV, consistent with the observational evidence that in NGC 5252 no ionizing photons are escaping in the line of sight.

Radiation-dominated (RD) clouds within that range of F_H intensities show velocities less than 250 km s^{-1} (cf. Viegas-Aldrovandi & Contini 1989, Fig. 1). Under these conditions, the detection in the nuclear spectrum of NGC 5252 of lines from high ionization levels, such as [Fe X], [Ne V][4] and possibly [Ar IV],[5] along with the low observed [O III] λ5007/λ4363 line ratio cannot be explained by "pure" photoionization models, as we shall see in § 5.2. An additional ionizing mechanism is required, and we propose shock heating. It is argued that shock-dominated clouds with velocities larger than 300 km s^{-1} can efficiently contribute to increase the gas temperature and to produce the high ionization levels that are observed.

The presence and central location of high-velocity clouds are supported by several observational results. The gas kinematics in the central region largely departs from ordered motion. Both neutral and ionized gas show their maximum velocity amplitudes $\sim$300 km s^{-1} in the inner few arcseconds. Redshifts and blueshifts with respect to the systemic velocity coexist in the central region in a random pattern (Prieto & Freudling 1996). Furthermore, the [O III] λ5007 line emission is reported by Held et al. (1992) to be double peaked in the nucleus. Acosta-Pulido et al. (1996) confirmed this by measuring broad and asymmetric profiles in the [N II], Hα, and [S II] lines, with FWHM of $\sim$400 km s^{-1}. Nelson & Whittle (1995) derived a gas velocity dispersion of $\sim$450 km s^{-1} in the central 1".5 × 2".5 region from their [O III] λ5007 line spectroscopy.

Summarizing, the following scenario for NGC 5252 is proposed. We expect the NLR clouds in NGC 5252 to be exposed to a composite power-law nuclear radiation with spectral indices $\alpha_{UV} = 1.5$ and $\alpha_X = 0.4$, and flux at the Lyman limit F_H about 10^9 cm^{-2} s^{-1} eV^{-1}. Moreover, high-velocity clouds ($V_s > 300$ km s^{-1}) contribute to the central gas heating. Since the ionizing nuclear flux is relatively weak, the high-velocity clouds tend to be shock dominated, whereas the low-velocity ones tend to be radiation dominated.

5.2. *Model Results: The Line Spectrum*

The observational data, reddening corrected, are listed in Table 1 (cols. [2] and [3]) and compared with model results (cols. [4]–[8]). All the line intensities are relative to Hβ = 1 to permit a better discussion of theoretical models.

The observations show [S II] λ6717/λ6731 $\geq$ 1, which indicates rather low densities in the emitting gas, while the low $R_{[O\,III]}$ (=[O III] λ5007/[O III] λ4363) ratio indicates high densities and/or high temperatures. Moreover, the presence of a nonnegligible [Fe X] line indicates a strong photoionizing radiation flux from the AC and/or high temperatures of the emitting gas. Therefore, a single model cannot fit the whole spectrum. We have run a grid of models with input parameters in the ranges given by the observational evidence and selected the best-fitting models or the models whose contribution can improve the fit of some particular lines in the averaged spectrum. Each composite model (which contains the effects of both the photoionizing flux and the shocks) is characterized by a different stratification of the ions, i.e., the ions correspond to different physical conditions and to different volumes of emitting gas.

Models R1, R2, and R3 are radiation dominated. Model R1 is characterized by input parameters as close as possible to the observational evidence. A higher intensity of the photoionizing flux will enhance the high-level lines and reduce the neutral and singly ionized lines in the spectrum because the clouds are not radiation bound. On the other hand, a lower flux corresponds to very low [O III] λ5007/[O I] λ6300 line ratios compared with the observations. Model R1 shows a good fit for most of the lines, except [Ne V], [O III] λ4363 and [Fe X] line ratios that are still unfit. Changing the other parameters will not improve the general agreement. Strong [Ne V] and [Fe X] lines and low $R_{[O\,III]}$ ratios are generally obtained in shock-dominated models with shock velocities higher than those considered in model R1. The input parameters of the shock-dominated model S1, which appears in Table 1 (col. [7]) are chosen in order to improve definitively the fit to the observed data. Interestingly, the observed FWHM of some line profiles (cf. § 5.1) is about the value indicated by model S1. High-velocity clouds are usually associated with high densities; thus n_0 above 200 cm^{-3} are assumed in the SD model. The higher the value of V_s, the higher the postshock compression and the higher the temperature of the gas in the postshock region, so SD models show low [S II] λ6717/λ6731 and low [O III] λ5007/λ4363 ratios.

The weighted sum of R1 and S1 spectra (model AV1) gives the best fit to observations and is listed in Table 1 (col. [10]). The relative weights appear at the bottom of Table 1 (W1) and show that R1:S1::1:2. The summed line ratios are within the observational error except for [Fe X], which is higher than the observed value by a factor of 10. Considering the absolute Hβ flux, R1 contributes about 88% and S1 12% of the observed flux. The fit of a model to the line spectrum is constrained by the fit of the spectral energy distribution of the continuum. Therefore, the validity of the model corresponding to AV1 will be further discussed in the next section.

Let us consider other cases that give acceptable results as well (cf. Table 1). It has been suggested that a series of clouds with different densities and velocities characterizes the NLR of Seyfert galaxies. In particular, lines from the same species receive different contributions from the various clouds (e.g., Filippenko 1985). The flux of Hβ increases by more than 2 orders of magnitude for $n_0 > 10^4$ cm^{-3}, which corresponds to a downstream $n > 10^6$ cm^{-3}. Line intensities increase with n^2. Then, if clouds characterized by high densities ($\geq 10^6$ cm^{-3}) contribute to the spectrum, their contribution dominates, i.e., all the line ratios should be characteristic of high densities. Particularly, $R_{[O\,III]}$ will be low, but [N I], which has a low critical density for collisional de-excitation (1.3×10^3 cm^{-3}) will be too weak to be observable (cf. Contini 1997, Fig. 6). This is not consistent with the spectrum of NGC 5252. Moreover, the presence of very dense gas will not improve the fit of high-level lines (e.g., [Fe X]) (Viegas-Aldrovandi & Gruenwald 1988).

A model with a higher density and a higher velocity (model R2) shows high [Ne V]/Hβ and [O III] λ4363/Hβ line ratios, but neutral lines are overpredicted. [Fe X]/Hβ is

[4] *HST*/WFPC filter imaging of NGC 5252 reveals the [Ne V] line to be possibly extended (Tsvetanov et al. 1996a, 1996b)

[5] Acosta-Pulido et al. (1996) mention the detection of [Ar IV] in the nuclear spectrum; however, no flux is reported.

still negligible. Note that in order to have a low $R_{[O\,III]}$, higher shock velocities are assumed. Velocities between 120 and 140 km s^{-1} correspond to temperatures in the post-shock regions up to greater than 2×10^5 and 3×10^5 K, respectively. The contribution of the hot gas in the post-shock region is important because, as already discussed, very high densities cannot be present in NGC 5252 (observed [N I] and [S II] are strong).

We have checked the case of a strong photoionizing flux that produces a strong [Fe X] line. Model R3 (Table 1) was run with F_H slightly higher than predicted in the previous section. The neutral lines and the singly ionized lines are negligible because the model is matter bound and the gas is maintained at a high temperature throughout the whole cloud by the primary and the diffused radiation. The [Fe X]/Hβ line ratio is about the observed value.

Both conditions invoked to improve the fit of model R1 (high density and high F_H) cannot coexist in a single model. In fact, a high density (increased also by compression downstream) causes rapid cooling of the gas and fast recombination. Therefore, the high-level lines become low and [Fe X], particularly, negligible, even when a large geometrical thickness of the cloud is adopted.

At the bottom of Table 1 the weight factor, W2, is given for each of the models. The weighted spectrum (AV2) appears in Table 1, column (11). Indeed, the input parameters of the models presented in Table 1 can be changed within small ranges without drastically changing the good fit of the calculated spectrum. It can be noticed that model R1 strongly prevails. Considering the absolute Hβ flux, we see that about 74.2% is due to model R1, 11.6% to model R2 (the high-density model), 13.9% to model R3 (the high-flux model), and only 0.25% to model S1 (the shock-dominated model).

In conclusion, the spectrum is well fitted by radiation-dominated clouds with relatively low n_0, low V_s, and a rather low F_H. However, the small contribution of denser clumps, of clouds reached by a stronger flux, and of shock-dominated clouds improves the fit of some weak lines. To fit the [S II] lines, the S/H relative abundance was reduced by a factor of 1.4 from the value in Allen (1973). This reduction was consistently applied in both radiation- and shock-dominated models.

The dust-to-gas ratio, d/g, derived from model R1 is low, $\sim 10^{-15}$, indicating that the central radiation does not suffer severe absorption in the NLR and can efficiently move outward in the bicone directions. The vale of d/g is about a factor of 10 larger in the SD model, which contributes most of the high-level lines. Since shock-dominated clouds tend to be closer to the central source, their high d/g points to a much larger extinction toward the central region. We shall come back to this point when discussing the continuum spectrum in the next section.

Further constraints to any of the proposed models can be obtained from the observed spectral energy distribution (SED) of the continuum.

5.3. *Model Results: The Continuum Spectrum*

5.3.1. *Sources of Continuum Emission in NGC 5252*

The various contributions to the continuum emission in NGC 5252 are briefly discussed below. The observed X-ray continuum emission above 1 keV is assumed to arise entirely at the central source and to be severely absorbed below that frequency. Thus, the continuum emission in the UV-optical region is expected to be due mainly to bremsstrahlung.

Kotilainen & Prieto (1995) showed that the main contribution to the optical continuum emission, and to a lesser extent to the near-IR, is of stellar origin. This contribution was shown to be dominant at optical wavelengths and progressively decreasing toward the near-IR. We found that a blackbody spectrum with $T = 3 \times 10^3$ K fits reasonably well the shape of the observed optical to near-IR continuum region (Figs. 1*a*, 1*b*, and 1*c*), and have adopted it as representative of the stellar contribution to the total nuclear emission. The precise amount of stellar light contributing to the central emission is in our case a model prediction and will be discussed below.

The IR continuum is assumed to be due to dust reprocessing. Because no outgoing star formation is detected in NGC 5252 (see § 3), the light contribution to the IR/*IRAS* is assumed to be essentially of nuclear origin.

5.3.2. *Shock-dominated and Radiation-dominated Continuum Models: AV2 Model*

The fit to the NGC 5252 line spectrum (§ 5.2) suggests that two main types of models are equally acceptable. Both include RD and SD clouds, but one (AV2) includes also dense clumps and clouds reached by a relatively strong radiation flux.

In Figure 1*a* the observed SED is compared with the SED resulting from model AV2 with relative weights W2 as indicated in Table 1. The trend of AV2 is essentially defined by models R1 and S1; the relative contributions of models R2 and R3 are at least a factor of 10 lower. Model R1 dominates the optical, far-IR and radio emission, whereas S1 contributes to the UV–X-ray and near-IR regions.

The continuum emission is essentially bremsstrahlung. In particular, model R1 accounts for the optical continuum and strictly relates to the "pure" nonstellar nuclear emission; thus, it predicts lower flux levels than observed. From the comparison between the observed and predicted values, the observed near-IR to optical continuum level is roughly a factor of ~ 10 larger than that derived from the model (Fig. 1*a*). By scaling the observed values down by this factor, the resulting near-IR to optical continuum shape and UV upper limit are found to fit remarkably well the continuum calculated by model R1. The current predicted nonstellar fluxes in the optical region are in fair agreement with Kotilainen & Prieto's upper limits derived for the same spectral region. The discrepancy is, however, larger in the mid-IR. In this region Kotilainen & Prieto's nonstellar fluxes are found to increase with wavelength, whereas the opposite trend is found here.

In addition to bremsstrahlung, collision and radiation heating of dust gives rise to peaked emissions in the far-IR region. Accordingly, model R1 accounts for the observed far-IR and respects the upper limit submillimetric data. The d/g value in the RD clouds is mainly determined by the continuum upper limits in the submillimeter range. The derived d/g is also an upper limit. Because the submillimetric region traces the cool dust emission, this should be placed at the outskirts of the nuclear region. The low d/g derived in RD models would thus be consistent with the low extinction measured from the Balmer decrement (note that the ratios of the Balmer lines are essentially measurements of the foreground, screen, and extinction).

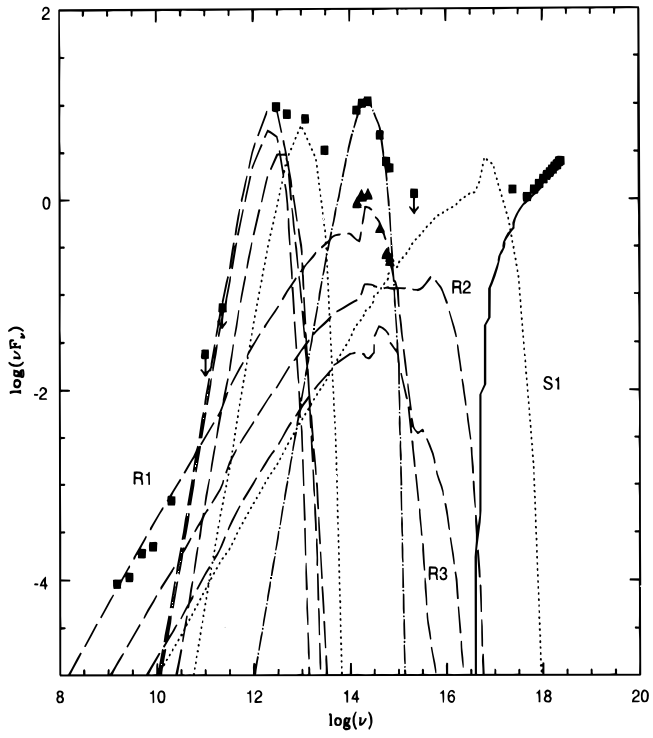

FIG. 1a

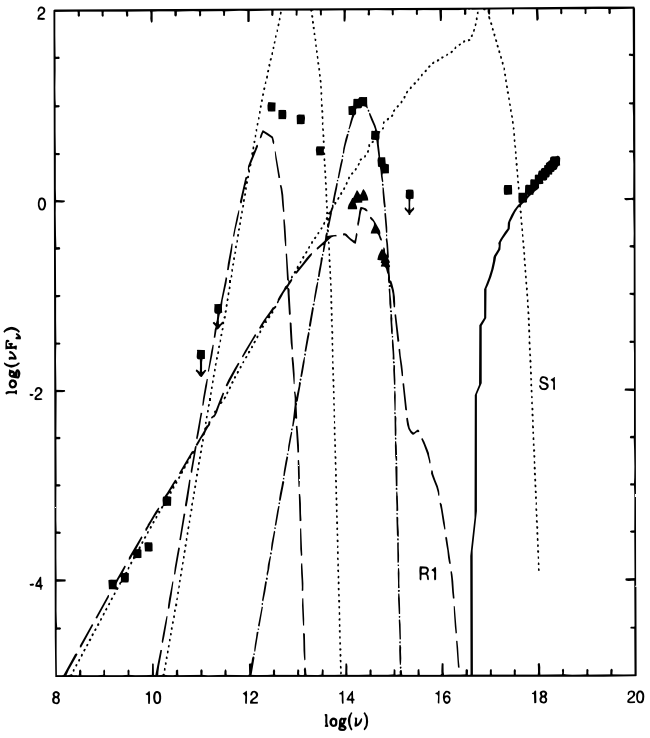

FIG. 1b

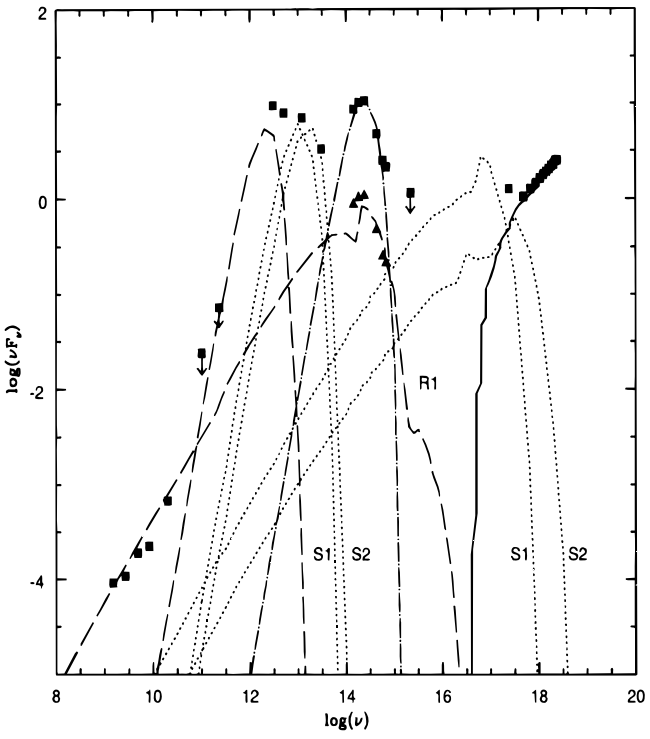

FIG. 1c

FIG. 1.—(*a*) AV2 continuum model for NGC 5252. Long-dashed lines refer to models R1, R2, and R3, and dots refer to model S1. The relative contributions of the models are given in Table 1. Note that for each model two separate distributions are shown: the gas continuum emission and the IR dust reprocessing emission. A thin solid line refers to the nuclear emission. The observational data are indicated by filled squares (and upper limits by arrows), the stellar-subtracted data by filled triangles. The dot-dashed line corresponds to a blackbody with $T = 3 \times 10^3$ K; νF_ν is in units of ergs cm^{-2} s^{-1}, and ν is in Hz. (*b*) Same as (*a*), but for models R1 and S1 with relative weights as defined by model AV1 (Table 1). (*c*) Same as (*a*), but for models R1, S1, and S2 with relative weights as defined by model AV3 (Table 2).

Velocities larger than 300 km s^{-1} in SD models correspond to gas temperatures in the postshock region above 3×10^6 K. This leads to an emission peak in the UV–X-ray zone. The peaked emission in the soft X-ray predicted by model S1 would then be consistent with the observed soft X-ray excess seen in the *ASCA* spectrum of NGC 5252, and provides an alternative explanation to the reprocessing scenario proposed by Cappi et al. (1996).

The corresponding heating of dust to those high temperatures gives rise to peaked emissions in the mid-IR

region. The higher the temperature of the gas, the higher the temperature reached by the dust grains. Yet grains cannot survive sputtering for a long time, so in high-velocity models dust emission is absent from the cool downstream region. Thus, the IR bump predicted by high V_s models is rather narrow. In particular, model S1 predicts a peak emission between 10^{12} and 10^{13} Hz that reasonably accounts for the observed SED in that region. The d/g value in the SD models is mainly determined by the mid-IR data. In this case the ratio is about 1 order of magnitude higher than that derived from RD models. Since shock-dominated clouds are expected to be located closer to a central active source, a larger d/g would imply a large dust concentration toward the central region. This scenario would thus be consistent with the observed increasing extinction toward the nuclear region of the galaxy (Kotilainen & Prieto 1995).

5.3.3. *Other Models*

Figure 1*b* shows the SED corresponding to model AV1. In this case, the relative weights are R1:S1::1:2, so that S1 dominates. The comparison with the observed data shows that even if AV1 is scaled up by a factor of 100 to match the observed levels, there are clear disagreements between the predicted and the observed SED shape. Note that, S1 being the dominant contributor, the predicted optical continuum trend turns to be difficult to reconcile with the observed one. Furthermore, the far to mid-IR continuum distribution appears inverted compared to what is observed.

A third SED model is presented in Figure 1*c*. In this case an additional shock-dominated model with $V_s = 1000$ km s^{-1} (model S2 in Table 1) is weight-averaged with models R1 and S1. Model AV3 provides the best simultaneous fit to the line and continuum spectra when the following relative weights (W3) are adopted: R1:S1:S2::100:5:0.02. The line spectrum derived from AV3 is given in the last column of Table 1. For comparative purposes, the weighted average of the two shock-dominated models S1 and S2 is also given (col. [9] in Table 1).

As was the case for model AV2, model AV3 is predominantly radiation dominated, since most of the line ratios are already well reproduced by model R1. However, the high-ionization lines, [Fe X] and [Ne V] are substantially increased because of the SD contribution; yet the [Ne V]/Hβ and [O III] λ4363/Hβ line ratios remain below the observed values. The results could be improved by adopting higher weights for the SD models, but this would spoil the fit to the continuum in the way it was attempted to evidence with former AV1 model.

In Table 2 the integrated fluxes at the different wavelength domains are given for models R1, S1, and S2. Note that the strongest X-ray emission is emitted by gas heated downstream by the high-velocity shocks.

TABLE 2

INTEGRATED FLUXES

Parameter/Region	R1	S1	S2
V_s (km s^{-1})	100	450	1000
n_0 (cm^{-3})	100	200	300
F_H (10^9 cm^{-2} s^{-1} eV^{-1})	4	0	0
d/g (10^{-15})	2	10	20
D (10^{18} cm)	1.5	>0.2	>29
Radio (10^7–10^{11} Hz)	1.4×10^{-5}	5.9×10^{-6}	3.4×10^{-4}
IR dust (10^{10}–10^{14} Hz)	0.078	1.72	409.
IR (10^{12}–10^{14} Hz)	0.012	0.011	0.49
Optical (3×10^{14}–10^{15} Hz)	0.0054	0.011	0.44
UV (10^{15}–5×10^{15} Hz)	0.0039	0.05	1.83
X-ray (>10^{17} Hz)	4×10^{-11}	0.65	57.3

5.4. *Model Implications*

Among the various models discussed above, model AV2 provides the closer representation to the observed line and continuum spectra. According to this model, the observed radio emission and the stellar subtracted optical continuum are due to bremsstrahlung. The infrared data are accounted for by dust heated by the central radiation (far-IR) and by shocks (mid-IR). Finally, the soft X-ray excess is explained by high-velocity shocked clouds. The low dust-to-gas ratio, derived from model R1, $\sim 10^{-15}$, indicates that the central radiation does not suffer severe absorption in the NLR and can efficiently move outward in the bicone directions. The dust-to-gas ratio is about a factor of 10 larger in the SD model. Since shock-dominated clouds are expected to be closer to the central source, their high d/g values point to a much larger extinction toward the central region, in conformity with the obscure nature of NGC 5252 Seyfert nucleus.

A rough estimate for the location of the high-velocity clouds could be derived from model S1 energy budget. The measured soft excess luminosity by Cappi et al. (1996), $L_X(0.1\text{–}2\ \text{keV}) = 9.7 \times 10^{40}$ ergs s^{-1}, can be compared with the corresponding contribution by model S1 (bottom of Table 2). Assuming a covering factor C for the clouds, and R being the nuclear distance to the SD clouds, we have $4\pi R^2 C(0.65 \times 5) = L_X$, which leads to $R(C)^{1/2} = 16$ pc. Thus, the region characterized by higher velocities would be located in the inner NLR.

As a final check, the size of the NLR could be estimated from the free path length for the ionizing photons in the NLR. The free path length, l, can be derived from the observed nebular extinction and the model-derived dust-to-gas ratio. The Balmer decrement sets a limit to the optical extinction of $A_\lambda = 1.086\tau_\lambda$ ($\sim$1 mag at V). The optical thickness at λ can be expressed as $\tau_\lambda = Q_{\text{ext}}\pi a^2\ n(\text{grain})\ l$, where Q_{ext} (the efficiency factor for extinction) = 2; a is the grain radius ($= 2 \times 10^{-5}$ cm), and n(grain) is the grain density by number [$= d/g \times n(\text{gas})$], with $n(\text{gas}) = 100$ cm^{-3} and $d/g = 2 \times 10^{-15}$ (see Table 1). With these values, the path length (or size of the NLR) is $l = 10^{21}$ cm (less than 1 kpc).

6. MODELING THE EXTENDED EMISSION-LINE REGION

All current observations for NGC 5252 support the idea that the gas in the bicone has a direct view of the central source and is thus ionized by the outflowing nuclear radiation. Thus, modeling of the extended emission-line region (EELR) was performed *on the basis of the just derived NGC 5252 nuclear model.*

Spectroscopy of the EELR in NGC 5252 was obtained in two position angles by Acosta-Pulido et al. (1996), and we used their data for our modeling purposes.

First, the density in the EELR clouds was derived. Because the only source of ionizing photons for the EELR is the nucleus, the previously derived nuclear flux F_H (Table 1) was considered as the available energy source for the EELR clouds. Also, the nuclear ionizing spectrum defined in § 5.1 is used as the input ionizing radiation spectrum for the EELR models. An estimate of the ionization parameter U was derived from the observed [O III]/[O II] line ratio at different regions in the nebula. $U \sim 10^{-3}$ was found

TABLE 3

EMISSION-LINE SPECTRA IN THE EELR

	Region									
	NW2 (22)		NW1 (8)		SE2 (9)		SE3 (15)		SH15 (15)	
Line/Parameter	Obs.	Calc.	Obs.	Calc.	Obs.	Calc.	Obs.	Calc.	Obs.	Calc.
[O II] λ3727	38 ± 12	41	46.7 ± 2.6	45	31.6 ± 3.2	29	34 ± 4	41	36 ± 4	40
[Ne III] λ3869.....	...	8	12.4 ± 1.2	8	8 ± 5	7.3	13 ± 4	7.5	10 ± 2.5	7
He II λ4686.....	...	...	...	...	...	...	...	...	2.9 ± 2.4	2.7
Hβ	11 ± 9	13.6	10.5 ± 3.5	14.5	9.5 ± 3.3	10	9.1 ± 1.6	13.5	9 ± 2.1	13.5
[O I] λ6300	...	5.7	5.7 ± 0.6	5.4	4.8 ± 1	5.7	4.5 ± 0.4	4.9	2.5 ± 2	2.4
[N II] λ6584	16.5 ± 1.9	17	22.7 ± 1	19	11.3 ± 1.3	11.8	19.5 ± 1.2	16.7	15.6 ± 0.9	15.5
[S II] λ6717	14.3 ± 1.8	7.6	11.4 ± 0.7	8.3	10.1 ± 1.5	5	8.8 ± 0.6	7.3	7.6 ± 0.5	6.3
[S II] λ6731	6.5 ± 0.9	5.2	6.6 ± 0.6	5.6	7.9 ± 1.2	3.4	6.6 ± 0.7	4.9	5.1 ± 0.3	4.3
n (cm^{-3}).....	...	2	...	2	...	2	...	2	...	2
U (10^{-3}).....	...	2	...	1.8	...	3	...	2	...	2
D (10^{20} cm)	...	2.4	...	1.9	...	4.3	...	2	...	1.2

NOTE—Regions are labeled following the nomenclature of Acosta-Pulido et al. 1996. The respective distances to the nucleus are indicated below the names of the regions. Only those regions for which a sufficient number of lines were reported are modeled. Line fluxes reported as upper limits were not modeled. Line ratios are relative to [O III] λ5007 = 100; line fluxes reported as upper limits were not modeled. Listed at the bottom are the parameters n (the electronic density), U (the ionization parameter), and D, the size of the emitting cloud.

roughly constant along the nebula ([O III]/[O II] does not vary much). An estimate of the density in the EELRs was derived from the proper definition of the ionization parameter, $U = F_{EELR}/(nc)$, where c is the speed of light, n is the cloud density, and F_{EELR} is the incident flux in a particular region within the bicone. F_{EELR} was derived from F_H after correction by the corresponding dilution factor. For the farthest regions in the bicone (∼20″–30″ from the center), the dilution factor within the solid angle defined by the bicone[6] is about 50–90, which leads to densities of ∼2–1 cm^{-3} at those distances. Note that on the basis of the observed [S II] line ratios, which are larger than the theoretical limit (Osterbrock 1989), only an upper limit of ∼100 cm^{-3} can be derived.

Once the ranges of densities in the EELRs were established, modeling of the line spectrum was attempted. Initially composite shock-photoionization models of the type described for the nucleus were used. The line profiles in the EELR appear unresolved at the spectral resolution achieved by Acosta-Pulido et al. (1996) (FWHM ∼90 km s^{-1}). Thus, shock velocities below that value were considered. With those input parameters, composite models were found to systematically produce shock-dominated spectra, even if velocities as low as 40 km s^{-1} were considered. The reason for this behavior resides in the relative low value of the nuclear flux F_H, and in turn of F_{EELR}, which leaves little room for photoionization to play a role in the presence of shocks. It follows that the predicted [O II]/[O III] ratio is always larger than the observed values because of the substantial increase of the O^+ zone via shocks. This result leads to the conclusion that *shock heating in the NGC 5252 EELR is negligible, the region being instead radiation dominated.*

Pure photoionization models were obtained with the photoionization code AANGABA (Gruenwald & Viegas 1995). This code is identical to SUMA for photoionization calculations, but it is faster.

As before, the nuclear ionizing spectrum and the dilution-corrected nuclear F_H were adopted as the input parameters at each region. Photoionization proved to be adequate to reproduce the observed line ratios as long as the emitting clouds have different optical depths at the Lyman limit (Viegas & Prieto 1992). Individual modeling for each of the observed regions is given in Table 3. Only those regions in the bicone with a sufficient number of lines and high signal-to-noise ratios were modeled. Those include regions NW2 and NW1 in the northern cone, and SE2, SE3, and SH15 in the southern one (the nomenclature of Acosta-Pulido et al. 1996 is followed).

The EELR clouds yield U-values between 1.8 and 2×10^{-3} when densities $n \sim 2$ cm^{-3} are assumed. The estimated size for the emitting regions varies between $2 \times 10^{20}$and 4×10^{20} cm, that being always smaller than the size of the observed integrated region. In general, a fair agreement between model and *individual* spectra is obtained. At each region, line ratios are reproduced within a factor of 1.3 or less, in particular when lines of high signal-to-noise ratio are involved. Major discrepancies are found for the [S II] lines at the farthest regions in the bicone: the models predict lower [S II] λ6717 line flux than observed. We note, however, that the observed [S II] line ratios in regions NW2 and NW1 (2.2 and 1.7, respectively) are far larger than the theoretical limit. The NW2 spectrum is particularly noisy (cf. Fig. 2 in Acosta-Pulido et al. 1996), and so we tend to believe that the reported flux errors are substantially underestimated.

7. CONCLUSIONS

Simultaneous modeling of the nuclear continuum energy distribution and of the line spectrum in NGC 5252 strongly constrains the fitting model. A composite model is proposed in which radiation-dominated gas accounts for most of the narrow-line emission gas and the low-frequency continuum, whereas dense clumps, highly illuminated clouds, and high-velocity clouds ($V \sim 400$ km s^{-1}) account for the [Fe X], [Ne V], [O III] λ4363 line emission, and the UV–soft X-ray continuum.

The infrared data are explained by emission from dust, which is heated by the central radiation and by shocks. The proposed composite model is consistent with the evidence that the impinging ionizing radiation in NGC 5252 is

[6] The cone angle of NGC 5252 is ∼75°.

severely absorbed, that being a key issue in the interpretation of the NGC 5252 anisotropic radiation field.

The comparison between models and observations yields a NLR region size of less than 1 kpc, with the high-velocity clouds being closer to the center by at least a few tens of parsecs.

The proposed composite model provides an alternative origin for the soft X-ray emission. Soft excess emission in AGNs is often interpreted as due to electron-scattered nuclear flux or thermal emission from the putative accretion disk. In the present context, high-velocity clouds naturally account for the soft excess component.

As a further step, modeling of the NGC 5252 extended emission-line region was performed on the basis of the nuclear model results. The density of the emitting clouds was found to be characterized by low values (a few cm^{-3}) and sizes of about 100 pc. Excitation via shocks is found to be negligible; instead, pure photoionization can fully account for the excitation of the gas as long as the emitting clouds have different optical depths at the Lyman limit.

We are very grateful to the referee for fruitful suggestions and constructive criticism, and to S. P. Willner for enlightening advice. We acknowledge FAPESP for financial support under grants 1996/6228-6 and 1996/6229-6. M. C. and M. A. P. thank the Instituto Astronômico e Geofísico (IAG) of São Paulo University for its warm hospitality.

REFERENCES

Acosta-Pulido, J., Vila-Vilaro, B., Perez, I., Wilson, A., & Tsvetanov, Z. 1996, ApJ, 464, 177
Allen, C. W. 1973, Astrophysical Quantities (London: Athlone)
Baldwin, J. A., Phillips, M. M., & Terlevich, R. J. 1981, PASP, 93, 5
Binette, L., Wilson, A., & Storchi-Bergmann, T. 1996, A&A, 312, 365
Cappi, M., Mihara, T., Matsuoka, M., Brinkmann, W., Prieto, M. A., & Palumbo, G. G. C. 1996, ApJ, 456, 141
Contini, M. 1997, A&A, in press
Contini, M., & Aldrovandi, S. M. V. 1983, A&A, 127, 15
———. 1986, A&A, 168, 41
Dopita, M., & Sutherland, R. 1995, ApJ, 455, 468
———. 1996, ApJS, 102, 161
Draine, B. T. 1981, ApJ, 245, 880
Dwek, E. 1981, ApJ, 247, 614
———. 1988, ApJ, 392, 814
Filippenko, A.V. 1985, ApJ, 289, 475
Gruenwald, R., & Viegas, S. M. 1995, A&A, 303, 535
Held, E. V., Cappaccioli, M., & Cappellaro, E. 1992, in AIP Conf. Proc., Testing the AGN Paradigm, ed. S. S. Holt, S. G. Neff, & C. M. Urry (New York: AIP), 613
Ho, L., Filippenko, A., & Sargent, W. 1993, ApJ, 417, 63
Korista, K. T., & Ferland, G. J. 1989, ApJ, 343, 678
Kotilainen, J. K., & Prieto, M. A. 1995, A&A, 295, 646
Maiolino, R., Ruiz, M., Rieke, G. H., & Keller, L. D. 1995, ApJ, 446, 561
Morse, J. A., Raymond, J. C., & Wilson, A. S. 1996, PASP, 108, 426
Mushotzky, R. F. 1982, ApJ, 256, 92
Nelson, C. H., & Whittle, M. 1995, ApJS, 99, 67
Osterbrock, D. E. 1989, Astrophysics of Gaseous Nebulae (Mill Valley: University Science Books)
Osterbrock, D. E., & Martel, A. 1993, ApJ, 414, 552
Pogge, R. 1997, in IAU Colloq. 159, Emission Lines in Active Galaxies: New Methods and Technique (San Francisco: ASP), 378
Prieto, M. A., & Freudling, W. 1993, ApJ, 418, 668
———. 1996, MNRAS, 279, 63
Stein, W. A. 1988, in Active Galactic Nuclei, ed. D. E. Osterbrock & J. S. Miller (Dordrecht: Kluwer), 201
Sutherland, R. S., Bicknell, G. V., & Dopita, M. 1993, ApJ, 414, 510
Tadhunter, C., & Tsvetanov, Z. 1989, Nature, 341, 422
Tsvetanov, Z. I., Morse, J. A., Wilson, A. S., & Cecil, G. 1996a, ApJ, 458, 172
———. 1996b, PASP, 105, 875
Veilleux, S., & Osterbrock, D. E. 1987, ApJ, 63, 265
Viegas-Aldrovandi, S. M., & Contini, M. 1989, ApJ, 339, 689
Viegas-Aldrovandi, S. M., & Gruenwald, R. B. 1988, ApJ, 324, 683
Viegas, S. M., & Contini, M. 1994, ApJ, 428, 113 (VC94)
———. 1997, in IAU Colloq. 159, Emission Lines in Active Galaxies: New Methods and Techniques (San Francisco: ASP), 365
Viegas, S. M., & Prieto, M. A. 1992, MNRAS, 258, 483